Sippl, C., Brisbout, L., Spaggiari, C. V., Gessner, K., Tkalčić, H., Kennett, B. L. N., Murdie, R. (2017): Crustal structure of a Proterozoic craton boundary: East Albany-Fraser Orogen, Western Australia, imaged with passive seismic and gravity anomaly data. - *Precambrian Research*, *296*, pp. 78—92.

DOI: http://doi.org/10.1016/j.precamres.2017.04.041

Crustal structure of a Proterozoic craton boundary: east Albany-Fraser Orogen, Western Australia, imaged with passive seismic and gravity anomaly data

C. Sippl[1,3], L. Brisbout[2], C.V. Spaggiari[2], K. Gessner[2], H. Tkalčić[1], B.L.N. Kennett[1], R. Murdie[2]

Abstract

We use passive seismic and gravity data to characterize the crustal structure and the crust-mantle boundary of the east Albany-Fraser Orogen in Western Australia, a Proterozoic orogen that reworked the southern and southeastern margin of the Archean Yilgarn Craton. The crustal thickness pattern retrieved from receiver functions shows a belt of substantially thickened crust that follows the trend of the orogen, but narrows to the southwest. Common conversion point profiles show a clear transition from a wide, symmetric Moho trough in the northeast to a one-sided, northwestern Moho dip in the southwest, where the Moho appears to underthrust the craton towards its interior. This change appears to coincide with the inferred trace of the Ida Fault, a major terrane boundary within the Yilgarn Craton.

Forward modelling of gravity anomaly data using the retrieved Moho geometry as a geometric constraint shows that a conspicuous, elongated gravity low on the northwestern side of the eastern Albany-Fraser Orogen is almost certainly caused by thickened Archean crust. To obtain a model that resembles the regional gravity pattern the following assumptions are necessary: high-density rocks occur in the upper crust of the Fraser Zone, at depth inside the Moho trough and in parts of the eastern Nornalup Zone east of the Moho trough. Although our gravity models do not constrain at which crustal level these high-density rocks occur, active deep seismic surveys suggest that large extents of the east Albany-Fraser Orogen's lower crust include a Mesoproterozoic magmatic underplate known as the Gunnadorrah Seismic Province.

The simplest interpretation of the imaged crustal structure is that the Gunnadorrah Seismic Province is underthrust beneath the Yilgarn Craton, likely as a consequence of crustal shortening during accretion further east. The imaged geometry overall appears to show a wedge of Archean lower crust that was driven between the exhumed Fraser Zone and the Gunnadorrah Seismic Province, effectively splitting the Paleo- to Mesoproterozoic crust of the east Albany-Fraser Orogen. The vertical splitting of Proterozoic crust by a cratonic crustal wedge, comparable to what we image in this study, may be a process that contributed to forming many craton margins around the world.

Keywords: Albany-Fraser Orogen, craton rim processes, Crustal thickness, receiver functions, gravity modeling, Western Australia

---

1. Introduction

Archean cratons, the oldest continental nuclei, are typically bound by Proterozoic orogenic belts that contain relatively thicker crust (Durrheim and Mooney, 1991; Mooney et al., 1998) and commonly lack deep, mechanically strong mantle lithospheric cratonic keels (e.g. James and Fouch, 2002). Thus, Proterozoic orogenic belts often act as weak "buffer zones" between the stable cratons, where mechanical and magmatic reworking events in response to tectonic reconfigurations preferentially focus (e.g. Black and Liegeois, 1993; Lenardic et al., 2000). In analogy to modern-day orogens, these orogenic belts can be subdivided into collisional and accretionary orogens (e.g. Cawood et al., 2009); the former are the result of a direct collision between two cratonic fragments, whereas the latter form in settings of protracted subduction and/or arc accretion along a craton margin. In many cases, an older accretionary event may be overprinted and/or consumed by a later collisional orogeny, for example the Gondwanan terranes in Tibet (e.g. Yin and Harrison, 2000).

In Australia, a continent where Archean cratons and Proterozoic orogens make up the western two thirds of the continental basement, a series of orogenic events during the Paleo- and Mesoproterozoic welded together three major cratonic blocks, the West, North and South Australian Cratons (e.g. Myers et al., 1996; Giles et al., 2004; Betts and Giles, 2006; Cawood and Korsch, 2008). Most of the Proterozoic orogenic belts between the cratonic cores are covered by locally thick sedimentary basins (Scott et al., 2000; de Vries et al., 2008), which has hampered direct access to basement rocks in these areas. The Albany-Fraser Orogen (AFO) is the southern and southeastern margin of the West Australian Craton, and its younger history corresponds with the latter stages of Mesoproterozoic continent assembly (e.g. Giles et al., 2004). Unlike some other Proterozoic orogens in Australia that have been identified as continental collisional belts (e.g. Tyler and Thorne, 1990; Johnson et al., 2011), the AFO appears to be an extensional accretionary orogen that, despite being modified by considerable crustal shortening, has never experienced continental collision with any other cratonic fragment. Evidence for this is provided by the magmatic and basin formation history as well as by the presence of oceanic arc type basement rocks in the Madura and Coompana Provinces east of the AFO, under the Eocene limestones of the Eucla Basin (Spaggiari et al., 2015; Spaggiari and Smithies, 2015; Smithies et al., 2015).

In this study, we combine two different geophysical approaches, passive source seismology and gravity analysis, to image the crustal structure of the east AFO. Receiver function analysis of data from a large temporary deployment of seismic stations in the southern two thirds of the east AFO yields a high-resolution

*corresponding author: sippl@gfz-potsdam.de; Deutsches GeoForschungsZentrum (GFZ), Am Telegrafenberg, 14473 Potsdam, Germany; Tel. +49-331-2881363

[1]Research School of Earth Sciences - Australian National University, Canberra, Australia

[2]Geological Survey of Western Australia, Perth, Australia

[3]now at: Deutsches GeoForschungsZentrum (GFZ), Potsdam, Germany

map of crustal thickness. Especially in old continental regions like Western Australia, where most surface topography has long been removed by erosion and where basement rocks are frequently buried under regolith or younger basin cover, Moho topography can provide important constraints on past tectonic processes (e.g. Kennett et al., 2011; Kennett and Saygin, 2015; Sippl, 2016). Previous studies around the world have shown a predominance of a flat and sharp Moho under most Archean cratons, but thickened, undulating, or gradational Moho topography has frequently been observed in adjacent Proterozoic terranes (e.g. Nguuri et al., 2001; Gilligan et al., 2016). This implies crustal thickening that is typically linked with continental collision or accretion. Preserved Moho character and topography are mostly indicative of past processes acting at lower crustal and uppermost mantle levels. Possible mechanisms for the creation of thickened crust include stalled subduction events (e.g. Mercier et al., 2008) as well as continental underthrusting and underplating. However, it is not always clear how accurately an imaged configuration represents the conditions at the time of orogeny since tectonic overprinting and modification can have obscured the region's initial signature. In the present study, we use the Moho topography that we retrieve from receiver functions as an input to gravity forward modeling. Subsurface lithology is inferred based on surface structural trends and the interpretation of three recently acquired whole-crustal seismic reflection profiles in the area (Spaggiari et al., 2014b). The resulting model of crustal structure is used as constraint to inform and modify existing models of the regional tectonic evolution.

2. Regional tectonic setting

The Albany-Fraser Orogen occupies the southern and southeastern margin of the Archean Yilgarn Craton in Western Australia (e.g. Myers, 1990), and represents extensive re-working of Yilgarn crust during the Paleo- and Mesoproterozoic (Kirkland et al., 2011; Spaggiari et al., 2014a, 2015). To the east, it is separated from the Madura Province by the Rodona Shear Zone (Figure 1A). To the west it is truncated by the Darling Fault and the late Mesoproterozoic to Neoproterozoic Pinjarra Orogen. Aeromagnetic and geochronology studies have shown that the AFO is continuous into the Wilkes Land region of eastern Antartica (e.g. Fitzsimons, 2003; Aitken et al., 2016), which implies that the Cretaceous rifting event (e.g. Gurnis, 1998) that separated Australia from Antartica occurred within the AFO.

The AFO was originally interpreted as a collisional orogenic belt that resulted from the amalgamation of the West and South Australian Cratons (e.g. Myers, 1993), the remnants of which are the Archean cores of the Yilgarn and Mawson (including the Gawler) Cratons. However, recent work on the AFO and the adjoining Madura Province has shown that the two cratons never met (Spaggiari et al., 2015; Spaggiari and Smithies, 2015). Thus, the Rodona Shear Zone, which separates the AFO from the Madura Province is the suture that separates modified Yilgarn crust from exotic (oceanic and oceanic-arc type) basement rocks under cover.

The Albany-Fraser Orogeny occurred in two tectono-thermal stages between 1330-1280 Ma and 1225-1140 Ma (Clark et al., 2000; Spaggiari et al., 2014a, 2015). Stage I is interpreted to have been triggered by the accretion of the Loongana Arc (Spaggiari et al., 2015), whereas Stage II is typically interpreted as reactivation and magmatism in an intracratonic setting. Before these orogenic events, the edge of the craton was a passive margin in a continental rift setting that evolved to form an ocean-continent transition from at least 1815 Ma to c. 1480 Ma (Spaggiari et al., 2015; Spaggiari and Smithies, 2015).

The NE- to NNE-trending east AFO is subdivided into two main units, the Northern Foreland and the Kepa Kurl Booya Province, which is further divided into the Tropicana, Biranup, Fraser and Nornalup Zones (Figure 1A; Spaggiari et al., 2014a): The Northern Foreland is separated from the largely unmodified Yilgarn Craton to the northwest by the Jerdacuttup Fault and the Cundeelee Shear Zone. Its Archean rock assemblages include the Munglinup Gneiss in the south (Figure 1; Myers, 1990; Spaggiari et al., 2014a,b). Southeast of the Northern Foreland, the Biranup Zone is dominated by deformed orthogneisses with ages between 1810-1625 Ma and includes Archean fragments of Yilgarn affinity (Spaggiari et al., 2014a; Kirkland et al., 2011). This unit extends along the entire length of the AFO, and is separated from the Fraser and Nornalup Zones by the Fraser, Newman and Coramup Shear Zones (Figure 1A).

The Nornalup Zone shares similar basement to the Biranup Zone, but hosts significant volumes of dominantly granitic intrusives defined as the 1330-1280 Ma Recherche and 1200-1140 Ma Esperance Supersuites, emplaced during the Albany-Fraser Orogeny (Smithies et al., 2015). Located between the Biranup and Nornalup Zones, the Fraser Zone is an approximately 450 km long, northeasterly trending belt of granulite facies metagabbros interlayered with granitic and sedimentary gneisses (Spaggiari et al., 2014a; Clark et al., 2014; Maier et al., 2016b) exhumed from mid- to lower crustal depths (Figure 1A). It is bound by the Fraser Shear Zone to the west and south, and the Boonderoo and Newman Shear Zones to the east, and was emplaced during Stage I of the Albany-Fraser Orogeny (Clark et al., 2014).

The Bouguer gravity map of the east AFO (Figure 1C) shows a pair of parallel anomalies (first reported by Fraser and Pettifer, 1980) that follow the trend of the orogen, a pronounced low in the west (referred to as Rason Regional Gravity Low in Fraser and Pettifer, 1980), coinciding with the transition from the Northern Foreland to the Biranup Zone. Directly east is the gravity high that clearly traces the mafic to ultramafic rocks of the Fraser Zone. Both of these anomalies fade towards the south, with the low continuing somewhat further south. With a high-to-low amplitude of $\sim$100 mgal, this pair of gravity anomalies are amongst the largest on the Australian continent; only the massive anomalies in Central Australia ($\sim$150 mgal) are significantly larger (e.g. Aitken et al., 2009; Kennett and Iaffaldano, 2013).

3. Data

We used passive seismic data from the recent temporary ALFREX (ALbany-FRaser EXperiment) deployment (Sippl et al., 2015), which yielded recordings from a total of 70 sites throughout the Albany-Fraser region between November 2013 and January 2016. In November 2013, 40 stations (24 short-period, 16 broadband) were installed in the northern part of the study area, in the region around and south of the 12GA-AF3 active seismic profile (Figure 5). About a year later, 27 stations were moved south (and augmented with an additional 3 short-period stations), whereas 12 of the 16 original broadband stations were left in place (see Figure 1). All ALFREX stations recorded 50 Hz continuous data onto local SD cards and were eventually retrieved in January 2016. The array was designed to cross all of the NE-SW trending tectono-stratigraphic units from the unmodified Yilgarn Craton in the west to the eastern Nornalup Zone to the east, the northern part of which is buried under cover of the Eucla Basin. The ALFREX dataset was complemented with data from two permanent stations located in the towns of Kambalda and Kalgoorlie, as well as the easternmost stations from the different WACraton temporary deployments in the years 2000-2001 and 2002-2004 (Reading et al., 2003; Goleby et al., 2006).

4. Methods summary

We employ P wave receiver function analysis in order to retrieve depth and geometry of subsurface discontinuities in seismic velocity (most prominently the Moho) as well as the distribution of bulk crustal v_p/v_s ratios. Time windows around teleseismic P phases for all earthquakes at suitable epicentral distances (30-95°) and magnitudes (M>5) were extracted (see Figure S1 in the Supplementary Material), and radial receiver functions were calculated using a time-domain iterative deconvolution technique (Ligorría and Ammon, 1999). An automatically pre-selected set of receiver functions for each station was checked visually, and traces that were too noisy were removed. Averaged raw receiver functions for all stations are shown in Figure S2. We then applied H-K stacking (Zhu and Kanamori, 2000; Chevrot and van der Hilst, 2000), a grid search approach to retrieve values of crustal thickness and bulk crustal v_p/v_s for each station from the addition of Ps, PpPs and PpSs amplitudes. Using the algorithm of Chen et al. (2010) and crustal v_p estimates from the AuSREM velocity model (Salmon et al., 2013), we allowed crustal thickness to vary between 25 and 65 km (0.1 km increment) and v_p/v_s between 1.6 and 1.9 (increment 0.005). All three phases were weighted equally. Figure S3 in the Supplementary Material shows examples of H-K stacking results for single stations. We determined uncertainties for H and K by bootstrap analysis (as in, e.g., Crotwell and Owens, 2005). 100 sets of receiver functions, each of them containing the same amount of traces as the original set (see Table S1), are randomly drawn with replacement from this original set of receiver functions (i.e. each trace can be drawn several times or not at all). Each of these 100 new sets is then used for calculating crustal thickness and v_p/v_s ratio. The standard deviation of the thus determined distribution is listed as the uncertainty value in Table S1. Additionally, we assigned quality classes A-D based on the sharpness of the H-K maximum (see examples in Figure S3) retrieved with the original set of receiver functions. The dependence of retrieved crustal thickness and v_p/v_s values on the input v_p value is visualized in Figure S4. Nine stations in the far eastern part of the array did not yield usable receiver functions due to strong reverberations induced by the slow sedimentary rocks of the Eucla Basin (Figure S5). For these stations, we retrieved a crustal thickness estimate from picking the Moho on autocorrelations (Gorbatov et al., 2013; Kennett et al., 2015) of ambient noise and P wave coda traces (see Figure S6 in the Supplementary Material). These stations are marked with a thicker circle outline in Figure 3A and with an asterisk in Table S1; no v_p/v_s values could be retrieved for these sites.

Additionally, we computed common conversion point (CCP) stacks for the selected receiver functions and projected them onto three profiles through the study area, using the global velocity model ak135 (Kennett et al., 1995) to convert times to depths and assuming horizontally oriented converters. The subsurface along the profile lines was subdivided into 2*2 km cells down to a depth of 200 km, and receiver function amplitudes were mapped into these bins.

5. Checking for Moho dip

Since we did not select events from narrow azimuthal and/or distance bins, our H-K stacking results can be affected if there is non-negligible Moho dip. Because receiver functions from different backazimuths are combined, the H-K stacking results represent a spatial average of crustal thickness over the area sampled by the RFs, with backazimuthal bins weighted by the number of traces from that bin in the total stack. To check for the presence of such contamination, we handpicked Ps-P times for all RFs and determined the median and inner quartile range of these time differences (Figure 2A). For stations that featured large inner quartile ranges of >0.5 s, we carried out a more detailed investigation of RFs (see two examples in Figure 2B). We concluded that there is substantial Moho topography under several stations, with Ps-P time differences of more than 1 second between receiver functions from different azimuth angles. Overlaying the Moho depth map retrieved from H-K stacking (Figure 3) onto these inner quartile ranges confirms that they are systematically larger in regions with a significant gradient in Moho topography.

To be able to image these variations among RFs of single stations, and thus to obtain a Moho depth map of higher spatial resolution, we also computed Moho depths at individual piercing points from Ps-P time picks for all single receiver functions, assuming a constant v_p/v_s of 1.73 and a crustal P wave velocity of 6.4 km/s. Although the retrieved 1,534 values of crustal thickness show significant scatter (Figure 4A), their smoothed interpolation together with Moho picks from active seismic profiles (Figure 4B) yields a map that is highly similar to the one retrieved from H-K stacking (Figure 3) in most areas, but resolves the narrow zone of thicker crust in the SW of the study area substantially better.

6. Results

6.1. Crustal thickness and v_p/v_s maps

A map of crustal thickness from H-K stacking is shown in Figure 3A; for the exact Moho depth values retrieved for each station refer to Table S1 in the Supplementary Material. The most prominent feature of the Moho depth map is a NNE trending trough of thicker crust that is continuous from the northern edge of our seismic array to the coastline in the south. This trough is already observable in the Ps-P times of the "raw" receiver functions shown in Figure S2. Stations on the unmodified Yilgarn Craton to the west uniformly show Moho depths of 35-40 km, and a similar subhorizontal Moho is imaged to the east of the trough, under the eastern Nornalup Zone. However, under the eastern Nornalup Zone the crust thickens from around 35 km in the southeast to about 40 km in the northeastern part of the array, where limestones of the Eucla Basin overlie the basement. A published crustal thickness value of 40 km at station FORT (Ford et al., 2010), about 200 km east of our array, indicates that the Moho continues nearly horizontally in that direction, beyond the study area.

The orogen-parallel trough reaches thicknesses of >45 km to the north, with a maximum value of 51.5 km obtained for station WR09 (Figure 3A), which is situated on the southern Fraser Zone. The Moho trough appears to narrow and exhibit shallower Moho depths (40-43 km) to the south (Figure 3). However, this shallowing is most likely an artifact of the limited lateral resolution of the H-K stacking map. In Figure 4, where we interpolated Moho depths from single receiver functions at their Moho piercing points rather than from station averages, the southern part of the Moho trough shows depths not significantly shallower than the northern part. This means that stations in the south that image the trough only do so for certain backazimuthal ranges (see Figure 2B).

An overlay of crustal thickness contours onto the regional Bouguer gravity map (Figure 5) shows that the Moho trough traces the gravity anomaly gradient, with the maximum crustal thicknesses situated around the transition from gravity low to high. In the northern part of the array, the maximum crustal thickness is imaged further west of the Fraser Zone, beneath the gravity low. To the south, where the gravity high of the Fraser Zone is absent, the deepest region of the Moho trough occurs at the eastern edge of the gravity low. Further south, where the gravity low has likewise disappeared, the Moho trough swings around to an ENE trend, possibly continuing subparallel to the coastline to the west of our array (Figures 4 and 5).

The P-to-S velocity ratio (v_p/v_s) values retrieved from H-K stacking are highest ($\sim$1.8) in and directly west of the Fraser Zone, which is displayed in Figure 3B with the red (positive) gravity contours. To the west of the Fraser Zone, there is a group of stations that gave quite low v_p/v_s (<1.7), whereas stations further west on the Yilgarn Craton yielded low to intermediate values of 1.71-1.75. South and east of the Fraser

Zone, we likewise retrieved intermediate v_p/v_s ratios, with the three easternmost stations showing higher ratios again. This may imply more mafic lithologies in the northern part of the eastern Nornalup Zone where it is overlain by the Eucla Basin, but a lack of data points from stations further east is problematic for such an interpretation. Moreover, there appears to be a tail of somewhat elevated values directly to the southwest of the Fraser Zone, following the general trend of the gravity anomalies.

6.2. CCP profiles

Figure 6 shows three CCP profiles that were constructed along lines perpendicular to the orogen's strike (see Figure 5), exploiting individual receiver function information with migration using the ak135 velocity model. In all three profiles, the Moho is clearly imaged as the most prominent negative (red) phase, whereas no other phases in the crust or uppermost mantle are continuously imaged across several stations. Absolute Moho depth values from these CCP profiles should be treated with caution, since the conversion to depth is performed using a global velocity model. However, crustal thickness differences between adjacent stations and thus the Moho geometry should be more accurately imaged.

All three profiles show a clear horizontal Moho beneath the Yilgarn Craton in the northwest and beneath the eastern Nornalup Zone in the southeast. The area of thickened crust between these regions, however, shows a clear progression in character from northeast to southwest. Profile A-A' shows a wide and symmetric Moho downwarp, with moderate dip angles on both sides, and the deepest point is located around kilometer 150, beneath the western part of the Fraser Zone (Figure 6). Further southwest, profile B-B' shows a narrower but deeper Moho trough, with steeper slopes on both sides. Additionally, the trough geometry is asymmetric, with a more steeply-dipping western side compared to the moderate dip on the eastern side, which is similar to that in profile A-A'. The dipping Moho on the eastern side appears to truncate that on the western side, with the latter's dip angle steepening towards that truncation (Figure 6, profile B-B'). Finally, profile C-C' shows a purely one-sided geometry, with the Moho of the eastern side showing a constant northwestward dip, whereas the Moho of the western side is imaged as purely horizontal, with no crustal thickening detected. Hence, a substantial Moho step of ∼15 km or more, from shallow in the northwest to deep in the southeast, is present under this part of the AFO. That this step appears larger in the CCP profile than the Moho depth difference at the same location seen in the Moho maps (Figures 3A and 4B) is due to the smoothing in these maps. It is important to note that no "double Moho" is imaged in this last profile, i.e. no shallower Moho, but rather a Moho gap is shown above the westward dipping, eastern Moho segment.

The thickest crust is found beneath the surface locations of the western part of the Fraser Zone and the adjacent Biranup Zone in profiles A-A' and B-B', and beneath the transition from Northern Foreland to Biranup Zone in the southwesternmost profile. This is consistent with the position of the Moho trough interpolated from the piercing points in Figure 5A. The western hinge line of the Moho trough, i.e. the position where the crust-mantle boundary starts to deviate from horizontal, is found at depth where the

Yilgarn Craton grades into the Northern Foreland at the surface, for profiles A-A' and B-B'. The eastern hinge line is found beneath the surface positions of the Fraser Zone's western end for profile B-B' and east of that, beneath the eastern Nornalup Zone, for profile A-A'. In profile C-C', which is situated where the orogen and the Moho trough acquire a more ENE trend, the SE end of the horizontal Moho on the cratonward side is situated beneath the Northern Foreland and the Biranup Zone boundary at the surface. The surface projection of the eastern hinge line in profile C-C' lies well within the Biranup Zone, which in this southern region is wider.

7. 2D gravity forward modelling

Paired gravity anomalies along Precambrian block boundaries have been observed and modelled for several locations inside the Australian continent (Wellman, 1978) and elsewhere (e.g. Gibb and Thomas, 1976; Gibb et al., 1983). In most studies, these anomalies were primarily explained with a density contrast between the craton and the adjacent younger (Proterozoic) orogen, with only a small variation in crustal thickness due to isostatic compensation. In this study, however, we can fix the crustal thickness to the values determined from receiver functions, and can thus better resolve the trade-off between crustal density distribution and Moho depth change for the AFO.

The relationship between the Moho trough that stretches along the Yilgarn Craton margin, the Bouguer gravity data and crustal structure were investigated by constructing 2D density models along sections A-A', B-B' and C-C' (Figures 1 and 5) and along active seismic lines 12GA-AF3 and 12GA-AF2. 2D gravity forward modelling was performed using Geosoft Oasis Montaj GM-SYS (v. 8.5). Gravity data, available with stations spaced in a $\sim$2 km grid and at 500 m intervals along active seismic lines, and SRTM topography data were sampled at 1 km intervals along all sections. Sections were modelled from the surface to a depth of 70 km and modelled units were extended past the ends of sections to avoid edge effects.

2D gravity forward modelling involves constructing a density model, comparing the gravity response calculated from the model to the observed gravity data, then iteratively making changes to the model until the calculated gravity adequately fits the observed data. A limitation of the method is that the results are non-unique; although a model may have a gravity response that adequately fits the observed data, it is just one of many possible models that will do so. Changes to the calculated gravity are the result of lateral density contrasts in the density model, thus lateral changes in the depth to the Moho, which juxtaposes denser upper mantle with less dense crust, produce long-wavelength changes in the calculated gravity data.

7.1. Simple Moho model

Initially, we constructed simple models with a uniform density crust overlying a homogeneous upper mantle. The crust was given a density of 2.67 g/cm^3 and the upper mantle a density of 3.20 g/cm^3. For sections A-A', B-B' and C-C', the Moho was constrained from the CCP profiles, for the other two profiles it was taken from the interpretation of the active seismic sections (Spaggiari and Occhipinti, 2014). In the CCP profiles, the Moho geometry is generally more angular than the smoothed Moho geometry interpreted from active seismic lines (see Figures 6 and 7).

A major feature of the observed gravity image is the northeast trending Rason Regional Gravity Low (Fraser and Pettifer, 1980) that stretches along the interface between the Yilgarn Craton and the AFO (Figure 1C). In gravity profiles, the Rason Regional Gravity Low is a comparatively more subtle feature due to its long wavelength and the superposition of other features, particularly Yilgarn Craton greenstone belts and, in sections 12GA-AF3 and A-A', the high density Fraser Zone. Along strike to the southwest, the Rason Regional Gravity Low grades into a relative gravity high, which is the dominant feature of the observed gravity in profile 12GA-AF2. A comparison of the observed and calculated gravity along sections A-A', B-B' and C-C' shows that the Moho trough produces a long wavelength gravity low (red lines in gravity plots of Figure 8). However, in profiles 12GA-AF3, A-A', B-B' and C-C' this gravity low is situated to the southeast of the trough, and in profiles B-B' and C-C', its amplitude is overestimated. In profile 12GA-AF2, the long-wavelength gravity low produced by the Moho trough is located on the observed gravity high situated along strike to the southwest of the Rason Regional Gravity Low.

7.2. Simple crustal density model

A better fit to the gravity data can be achieved by the addition of different crustal units to the density models. The geometries of the units were constrained from the interpreted bedrock geology map (Spaggiari, 2016) and the interpreted active seismic lines (Spaggiari and Occhipinti, 2014). In sections A-A', B-B' and C-C', the geometries of the different units were simplified and extrapolated along strike from the interpreted active seismic lines.

In the density models along sections 12GA-AF3, A-A', B-B' and C-C', the gravity low produced by the Moho trough was shifted towards the northwest by the addition of a dense crustal body (2.95 g/cm^3) inside the Moho trough. This dense body is coincident with non-reflective zones interpreted in active seismic lines 12GA-AF3 and 12GA-AF2 (Spaggiari and Occhipinti, 2014; Murdie et al., 2014), and might represent a mix of upper mantle and lower crustal material. In sections B-B' and C-C', the non-reflective zone is required to extend to the southeast beneath the Northern Foreland and Biranup Zone. This geometry is not consistent with active seismic interpretations that show the non-reflective zone with a symmetric geometry and occupying only the Moho trough and the Yilgarn Craton lower crust. To achieve a symmetric geometry and confine this dense body to the Yilgarn Craton and Northern Foreland lower crust, the density of the Biranup Zone upper and middle crustal rocks can be slightly increased in sections B-B' (2.70 to 2.725 g/cm^3) and C-C' (2.70 g/cm^3), which implies a density variation of that unit along the orogen's strike. To the southwest, following the trend of the orogen, the Rason Regional Gravity Low grades into the relative gravity high traversed by profile 12GA-AF2. The Moho trough in this profile is shallower and more gently dipping than to the northeast, although this might be an artifact of the method (active seismics vs. CCP stacking) or of the profile's orientation that is not perpendicular to the orogen's strike. A combination of a shallower Moho trough and a larger and shallower, dense lower crustal unit can produce the Bouguer gravity high along strike of the Rason Regional Gravity Low and observed in 12GA-AF2.

Another major feature of the Bouguer gravity data is the relative gravity high produced by the metagabbro dominated Fraser Zone. In sections 12GA-AF3 and A-A', a dense Fraser Zone and a dense unit to the southeast of the Fraser Zone are required to satisfy the observed Bouguer gravity highs. The Bouguer gravity image in Figure 1C, as well as the observed gravity profiles along sections 12GA-AF3, C-C' and 12GA-AF2, suggest that the crust of the AFO has a higher bulk density than the Yilgarn Craton. In our density models, this higher bulk density is accounted for by the Gunnnadorrah Seismic Province, a dense, moderately to strongly reflective lower crustal unit characterised by subhorizontal reflectors (Spaggiari et al., 2014b). Although density models of Sections A-A' and B-B' do not require a dense Gunnadorrah Seismic Province in the AFO, this unit has been included for consistency along strike. Alternatively, the upper and middle crust of the AFO can be modelled with above average densities.

In summary, a significantly better fit to the observed gravity data compared to the homogeneous crustal models (Section 7.1) is achieved by the addition of 1) a dense body in the Moho trough, 2) a dense Fraser Zone in the AFO upper crust, and 3) a dense Gunnadorrah Seismic Province in the AFO lower crust.

8. Discussion

In this section, we discuss possible interpretations of the obtained crustal configuration, first linking the obtained geometry to possible processes (Sections 8.1 and 8.2), and then evaluating whether and how these processes are compatible with the current knowledge of the regional tectonic evolution (Section 8.3). We discuss the special role of the Fraser Zone metamorphic rocks, and try to establish whether their exhumation can be related to the imaged geometries (Section 8.4), and finally try to establish whether the interpreted processes could be typical of craton margin processes worldwide (Section 8.5).

8.1. Geometric configuration and its possible origin

Our retrieved Moho geometry features a northward widening V-shaped Moho depression in the northern part of the study region and an abrupt transition to a one-sided, east-under-west configuration to the south (Figure 6,8). Continent-wide compilations of Moho thickness (Clitheroe et al., 2000; Collins et al., 2003; Kennett et al., 2011) as well as regional studies of Western Australia (e.g. Reading et al., 2007; Yuan, 2015) to date had a reasonable coverage of most of the Yilgarn Craton itself, but severely lacked resolution at the craton's edges, so that the presence of the Moho trough beneath the AFO we have imaged here was previously unknown. The active seismic profiles acquired in 2012 (Spaggiari et al., 2014b; Korsch et al., 2014) indicated thicker crust beneath the AFO, but due to their two-dimensionality, wide separation, and orientation in east-west direction (i.e. not always perpendicular to the orogen's strike, which leads to an underestimation of dip angles), they only provided limited information on the crust-mantle boundary geometry. Given the change in trend of the Moho trough recorded in the southern part of the ALFREX array, it appears possible that the observation of anomalously thick crust along an onshore-offshore active seismic profile further west (Tassell and Goncharov, 2006; Mjelde et al., 2013) is a continuation of the same structure. If this is correct, the Moho trough would wrap around the craton margin, potentially continuing within the AFO as far west as the Darling Fault, where the orogen is truncated by the Pinjarra Orogen. To the northeast, the pair of gravity anomalies discussed in Sections 2 and 7, which are in all likelihood caused by the presence of the Moho depression and the overlying Fraser Zone (Figure 8), are continuous as far north as the Tropicana Zone, where a short active seismic profile (12GA-T1, Occhipinti et al., 2014) also indicates the presence of an east-under-west configuration in the lower crust. An east-west profile at 32°N (Kennett and Yoshizawa, 2016) through a continent-wide surface-wave tomography model (Yoshizawa, 2014) shows a prominent westward shallowing of the LAB (lithosphere-asthenosphere boundary) at around 124°E, which is close to the location of the area of thickened crust we have retrieved. This could imply that the Moho trough is situated close to the transition to the cratonic mantle lithospheric keel of the Yilgarn Craton. The change in along-strike geometry of the Moho trough, from symmetric in the northeast, to asymmetric, to one-sided in the southwest (Figure 6), must reflect differences in the response of the crust and upper mantle to tectonothermal events. In the southwest, this is perhaps reminiscent of crustal-scale underthrusting. The transition to an offset in the Moho spatially coincides with the position where the Ida Fault, a major terrane boundary within the Yilgarn Craton, is inferred (Figure 1A). The Ida Fault is clearly visible as a distinct feature in aeromagnetic images further northwest, but in the southern Yilgarn Craton it is intruded by granites, and its trace within the reworked crust of the AFO is not clearly defined. Between the towns of Southern Cross and Kalgoorlie, the Ida Fault has been imaged with an active seismic profile as a ∼30° E-dipping normal fault (Swager, 1997) penetrating to lower crustal depths. We speculate that the Ida Fault, as a pre-existing zone of weakness, may have accommodated a regional difference in material strength or upper-lower plate coupling, which led to the localization of the observed Yilgarn-side offset.

8.2. Subduction or continental underthrusting?

Unlike the western side of the Moho trough, which changes its geometry significantly along strike, the eastern side is imaged as continuously dipping at a relatively constant angle (Figure 6). We see no indication of a descent of crustal material beyond the tip of the V in profiles A-A' and B-B', whereas profile C-C' shows a very faint indication of a throughgoing negative phase that could be interpreted as continuation of the downgoing eastern side Moho. However, this is far from being compelling evidence. In principle, a configuration such as that imaged can be achieved by an oceanic or continental subduction process or by continental underthrusting.

In a subduction scenario, even if a subsequent slab breakoff is invoked, the subducting slab would have to continue downdip beyond where we clearly image it. The observed lack of a substantial velocity contrast downdip could be the consequence of thermal and/or chemical modification of the downgoing material due to prolonged exposure to mantle material and high P-T conditions. Examples of receiver function imaging from ongoing oceanic (Pearce et al., 2012) and continental subduction (Schneider et al., 2013) show that downgoing crust on top of the slab is usually depicted as a low-velocity zone bound by two parallel anomalies of opposite sign, a negative one where the contrast from fast mantle to slow crust is encountered (lower edge) and a positive one above, where the opposite transition occurs. This feature is usually imaged as a direct continuation of the Moho of the downgoing plate. The fact that these anomaly pairs can only be imaged to depths of ∼60-100 km is due to mineral reactions (most importantly eclogitization, e.g. Wittlinger et al., 2009; Bostock, 2013) that increase the density and thus seismic velocity of the downgoing crustal material and eventually, upon completion of the transformation, make it indistinguishable from background mantle velocities. However, since these regions feature ongoing convergence at velocities in the order of >1 cm/yr, thermal and chemical/mineralogical assimilation of the slab (and the oceanic or continental crust above it) at depth is retarded, i.e. material is carried some distance beyond its equilibrium stability field before the reaction/assimilation is complete. The structure we image here, however, has in all likelihood been stagnant since about 1.1 Ga (based on the last recorded events in the AFO; see Section 8.3), thus subducted material would have had ample time to assimilate to mantle conditions.

If subduction is inferred, the variable geometric signature of the western (craton) side could be a consequence of differences in upper plate coupling. The absence of a shallower (double) Moho in profile C-C' (Figure 6) may be the consequence of mantle wedge serpentinization (e.g. Guillot et al., 2000; Bostock et al., 2002), which occurs as a consequence of slab dehydration and can lead to a substantial decrease of shear wave velocities in the mantle wedge. This has the effect of obscuring, sometimes even sign-flipping, the overlying continental Moho (Bostock et al., 2002), while still providing the high rock densities that appear to be required by the forward models (Section 7). Thus, the lower crustal dense body inside the Moho trough retrieved with the gravity forward models (Figure 8) could be interpreted as mantle wedge serpentinites if a subduction scenario is preferred. Although possessing high rock densities, serpentinites feature rather slow S wavespeeds (due to high $v_/v_s$ ratios), which would explain why their upper termination is not imaged in the CCP profiles. However, a possible signature of these hypothetical serpentinites in the bulk crustal v_p/v_s distribution we obtain (Figure 3B) would only be consistent with the northern part of the Moho trough, and even there it is not possible to distinguish whether the elevated v_p/v_s values come from lower crustal depths or from the upper crustal Fraser Zone rocks. However, aside from the fact that we do not clearly image a downgoing slab, its presence is also difficult to argue for geometrically. The Archean Yilgarn Craton to the west has an intact mantle lithospheric keel that has been imaged with continental-scale surface wave tomography (e.g. Yoshizawa, 2014) as extending to depths most likely exceeding 200 km. The presence of this keel, most likely formed during Archean processes prior to AFO tectonism, implies that there is not enough space for a slab subducting in a northwestward direction at this position, providing clear evidence against a major subduction zone setting at this locus. Moreover, geochemical and isotopic data, combined with basin analysis and structural considerations and the lack of any continental arc or subduction-related rocks argue against a subduction setting within the AFO, and beneath the craton margin (Spaggiari et al., 2015; Smithies et al., 2015; Spaggiari and Smithies, 2015). However, based purely on our images and purely geometrical considerations, it is feasible that a short-lived "failed" subduction event occurred, where the downgoing slab stalled soon after subduction initiation, possibly upon impingement onto the Yilgarn lithospheric keel.

An alternative interpretation of our observations is a model of continental underthrusting through crustal-scale wedge formation (also called "crocodile tectonics"; Meissner, 1989), i.e. the crust of the eastern side separated into an overthrust upper crustal section and a partially underthrust lower crust (in this case the Gunnadorrah Seismic Province, see Section 7, Figure 8). In such a configuration, frequently observed at accretionary margins (Snyder and Goleby, 2016), there is no need for a continuation of the imaged downgoing Moho to deeper depths, and a fit into existing tectonic models (Section 8.3) is easier to obtain. Moreover, the geometry of the units in the interpreted active seismic profiles, especially profile 12GA-AF3, is indicative of this process, with Yilgarn-related crust (Udarra Seismic Province) apparently splitting AFO-related units (Biranup Zone, Gunnadorrah Seismic Province) at mid-crustal levels (Figure 7; Spaggiari et al., 2014b). The upper crustal successions of the AFO could thus be a "flake" (Oxburgh, 1972) that got separated from its lower crustal part by the Yilgarn-side tectonic wedge. Since this horizontal crustal indentation is found between the AFO and Yilgarn Craton, i.e. between modified craton margin and unmodified craton, and not between craton margin and accreted oceanic arc further east, it could either have formed by inboard stress transfer from the accretion event (i.e. coeval with it) or at a later point in time (see also Section 8.3).
The observed absence of a double Moho in the southwest has to be explained differently in such a setting, since mantle wedge serpentinization can not readily be invoked without subduction, and continental material, even if submerged to sufficient depths, does not contain large enough concentrations of hydrous minerals to promote serpentinization at this scale. However, the regional gravity pattern features a gravity high on top of the Moho trough in the southwest of the ALFREX array, beyond where the anomaly pair discussed beforehand fades out (e.g. Figure 5B). This feature is hard to reconcile with substantially thickened crust, which should have the opposite signature. In the case of a continental underthrusting scenario, we thus have to explain the area between the middle to upper crust and the underthrust lower crust, imaged as lower

crustal non-reflective zones in active seismic profiles 12GA-AF2 and 12GA-AF3 (Figures 7 and 8), with a high-density crustal or mixed lithology, such as continental lower crustal rocks heavily intruded and/or modified by the underlying mantle rocks. Such a process has been interpreted from geochemical and isotopic data from gabbroic rocks of the Fraser Zone, where mantle melts have acquired small volumes of crustal material that was subsequently ponded in staging chambers, prior to intrusion (Maier et al., 2016b). It is feasible that the non-reflective zones within the trough may contain remnants from a similar process. A more mafic lithology compared to the overlying rock suites except the Fraser Zone (e.g. through intrusion by mafic mantle rocks) would effect a higher v_p/v_s ratio in this high-density lower crustal unit, so that although density and thus v_p are higher than for the overlying rocks, the S wavespeed difference could become small enough to not create a significant conversion phase that would show up in the receiver functions. The high-v_p/v_s tail we image trending southwestward from the southern end of the Fraser Zone (Figure 3B), along the deepest extent of the Moho trough, may be a signature of this lower crustal unit.

8.3. Implications for regional tectonic evolution models

Both subduction and "flake" tectonic processes that could have affected the current crustal configuration require an extended period of crustal shortening for their formation. Apart from the Tropicana Event, where the Tropicana Zone was thrust over the Yamarna Terrane of the Yilgarn Craton at c. 2520 Ma (Occhipinti et al., 2016), prior to Stage I of the Albany-Fraser Orogeny the AFO was dominated by extensional tectonics associated with continental rifting and basin formation, leading to formation of a passive margin and an ocean-continent transition (Spaggiari et al., 2015). These events may have been responsible for early manifestations of the crustal architecture imaged. Although further north than the ALFREX array, the Tropicana Zone is interpreted as an imbricate fan thrust northwestward along a crustal ramp (Occhipinti et al., 2016), potentially over a northward extension of the Moho trough described here. Rifting from at least 1815 Ma may have utilized the transition from strong Yilgarn Craton crust to modified AFO crust (Spaggiari et al., 2015). The major change to a compressive regime would have occurred during accretion of the Loongana Arc from the east by c. 1330 Ma, although the structural effects on the AFO of this event are not well constrained, i.e. it is not always clear whether thrust-related structures formed during Stage I or II of the Albany-Fraser Orogeny, or both (Spaggiari et al., 2014a,b).

Since the observed change in Moho trough geometry we observe spatially coincides with the presence or absence of the Fraser Zone, it is tempting to speculate that the lower crustal geometry we image may have facilitated its emplacement (see Section 8.4). If that is the case, the Moho trough formation had to predate or be contemporaneous with Fraser Zone emplacement. Another observation that may help constrain relative timing is that the Moho trough marks the boundary between regions of widespread magmatism during the Mesoproterozoic east of the trough, whereas to the west these intrusions are minimal, although high temperature metamorphism during these events was present. Mesoproterozoic intrusions belong to the

1330-1280 Ma Recherche and 1200-1140 Ma Esperance Supersuites (Smithies et al., 2015), and the 1192-1150 Ma Moodini Supersuite in the Madura Province (Spaggiari and Smithies, 2015). If the westward cessation of intrusive activity is indeed causally connected to the processes that produced the current trough geometry, then the formation of the Esperance and Moodini Supersuites is the latest possible time when this trough must have already been in place. Spaggiari and Smithies (2015) proposed that the Gunnadorrah Seismic Province (Figure 7) may have been the source area of these voluminous granitic intrusions into the upper crust. The Gunnadorrah Seismic Province would thus consist of relatively more mafic restites, i.e. remaining material after extraction of the felsic melts, which could explain the observations of high densities associated with the Gunnadorrah Seismic Province (Figure 8), and possibly the elevated v_p/v_s ratios towards the east of our array (Figure 3B).

8.4. Role of the Fraser Zone

The position of the western portion of the Fraser Zone metamorphic rocks directly above the deepest part of the Moho trough, as well as their absence on top of the one-sided geometry further south, is peculiar and strongly hints at a causal link. The current model for the emplacement of the Fraser Zone features a SE-dipping crustal ramp that may have facilitated intrusion (see Figure 23 in Maier et al., 2016a). Although the Fraser Zone rocks are dominantly mafic (Smithies et al., 2014), the geochemical and isotopic constraints show that their origin is not oceanic arc (Fletcher et al., 1991; Kirkland et al., 2014; Smithies et al., 2014), contrary to what has been proposed in earlier studies (e.g. Condie and Myers, 1999). It is thus possible that the SE-ward dipping Moho we image on the Yilgarn side (Figure 6, profiles A-A' and B-B') represents the lower end of this crustal ramp; in this case, the southwestward termination of the ramp near the Ida Fault would have defined the southwestward extent of the Fraser Zone, since emplacement would be less feasible in the absence of the ramp. At the same time, it is conceivable that the northward widening of the Moho depression, with the eastern hingepoint migrating further eastward towards the north (see profile A-A' in Figure 6), is due to crustal sagging induced by the load of high-density Fraser Zone rocks (see Section 7, Figure 8) in the upper crust. The presence of the positive gravity anomaly associated with the Fraser Zone indicates that a full isostatic compensation by crustal thickening underneath has not occurred, possibly due to the rigidity of the underlying mantle lithospheric material. However, a partial compensation leading to the wider area of thickened crust in the northern part of our array may have been achieved.

8.5. Implications for craton margin processes

The process of crustal wedge indentation has been proposed and imaged for a large number of recent convergent orogens (e.g. Teixell, 1998; TRANSALP_working_group, 2002; Moore and Wiltschko, 2004). The various models differ in detail, but nearly all of them show an upper plate crustal wedge splitting the crust of the lower plate along a weak horizon, usually above the lower crust. The lower crustal sliver, together with the underlying mantle lithosphere, is pushed to greater depth by ongoing plate convergence, experiences mineral reactions in the eclogite field and finally delaminates (Moore and Wiltschko, 2004). In a recent study, Snyder and Goleby (2016) evaluated a large number of global active seismic profiles, and found crustal wedge structures resembling the one we retrieved to be a relatively ubiquitous feature in accretionary orogens involving continental margins, irrespective of their age. One of their Proterozoic examples is situated in northeast Australia (Mt. Isa region, see Korsch et al., 2012) and resembles our findings to a large degree.

Most active seismic images from craton margins around the world show somewhat thickened crust compared to the craton itself as well as younger upper crust overthrusting over the craton's crust, but lack the downward dipping lower crustal unit that we imaged in the AFO (e.g. Lewry et al., 1994; Bayer et al., 2002; Hajnal et al., 2005; Zhang et al., 2014). This could imply that while the upper crustal "flake" is always preserved after cessation of the craton margin orogeny, the submerged lower crustal part usually detaches and founders into the mantle (e.g. Moore and Wiltschko, 2004), due to eclogite-facies mineral reactions and/or the inherently higher density of Proterozoic and Phanerozoic mantle lithosphere (Poudjom Djomani et al., 2001). In the AFO, a limited amount of total shortening could have led to an "incomplete" orogeny, with the lower crustal sliver still attached.
Most passive seismic studies of cratonic margins to date did not use dense enough arrays to image such local features in detail, but some have shown regional thickening of Archean craton crust towards the margin (e.g. Youssof et al., 2013; Yuan, 2015). This could hint at a process akin to what we see in the northern part of our array, where the Yilgarn side crust is bent downwards, possibly due to strong coupling to the downgoing Proterozoic side (Figure 6). That such marginward thickening of cratonic crust is not imaged everywhere perhaps indicates that local rheological variation controls whether Proterozoic or Archean tectonic units are thickened during crustal shortening. Even in the small area we illuminated in this study, there is an along strike change from presence to absence of thickened cratonic crust.

9. Conclusions

We used data from the temporary ALFREX seismic deployment to retrieve maps of crustal thickness as well as three CCP profiles perpendicular to the strike of the Albany-Fraser Orogen from radial P receiver functions, and forward modeled gravity profiles using this Moho geometry as input constraints. While the Yilgarn Craton in the west and the eastern Nornalup Zone in the east feature a constant crustal thickness of 35-40 km, a belt of significantly thicker crust (>45 km) was retrieved between these regions. The geometry of the thickened crust resembles a symmetric trough in the northern part of the study area. In the southern part, the eastern (AFO) side underthrusts the horizontal western side, south of the approximate position of the Ida Fault terrane boundary in the Yilgarn Craton. Gravity models show that the observed pattern of anomalies across the east AFO can be obtained by combining the retrieved crustal thickness distribution with high rock densities in the upper crustal Fraser Zone, a dense lower crustal body inside the Moho trough (interpreted as "non-reflective zones" in the active seismic profiles) and the lower crustal Gunnadorrah Seismic Province east of the Moho depression.

The retrieved geometry and density distribution suggests a process of crustal wedge indentation followed by lower-crustal underthrusting. The timing of such significant crustal shortening is unclear, but most likely relates to Mesoproterozoic thrust events recorded during Stages I or II of the Albany-Fraser Orogeny, perhaps facilitated by the pre-existing architecture. Options include shortening related to oceanic arc accretion from the east (Stage I), a later period of compression during formation of the Fraser Zone, and/or pulses of compression that produced widespread thrusting during prolonged Esperance Supersuite magmatism during Stage II. Although the imaged thickened crust could be interpreted as consistent with a continental subduction scenario, the lack of continental arc magmatism and subduction-related rocks within the orogen make this difficult to justify. Relatively dense, inferred mafic rocks in the lower crust can be accounted for as residual products from intrusive events that on the surface are clearly not subduction-related.

The along-strike change in behaviour of the (western) Yilgarn-side lower crust may be a consequence of differences in coupling between the two lower crustal units, and the resulting ramp geometry in the north may have provided the ascent pathway for the Fraser Zone metagabbroic rocks. In the south, where the Fraser Zone rocks are absent, the western side of the Moho trough is horizontal. The Albany-Fraser Orogen could thus represent the rare case of an orogen where an Archean crustal wedge split the adjacent Proterozoic crust, but where the lower crust of the Proterozoic side did not delaminate eventually.

Acknowledgments

We thank everybody who helped out on the numerous field campaigns (R. Addenbrooke, A. Arcidiaco, U. Azad, J. Byrne, S. Fanning, Q. Li, G. Luton, J. Maina, M. Mustać, T. Pejić, P. Sandow, K. Smith, J. Stephenson, C. Zirk), as well as the ANSIR instrument pool for the utilized seismometers and recording units. This research was funded through ARC Linkage Grant LP130100413. C.V. Spaggiari and K. Gessner publish with the permission of the Director of the Geological Survey of Western Australia.

References

Aitken, A.R.A., Betts, P.G., Weinberg, R.F., Gray, D., 2009. Constrained potential field modeling of the crustal architecture of the Musgrave Province in central Australia: Evidence for lithospheric strengthening due to crust-mantle boundary uplift. Journal of Geophysical Research 114, 1–23.

Aitken, A.R.A., Betts, P.G., Young, D.A., Blankenship, D.D., Roberts, J.L., Siegert, M.J., 2016. The Australo-Antarctic Columbia to Gondwana transition. Gondwana Research 29, 136–152.

Bayer, U., Grad, M., Pharaoh, T.C., Thybo, H., Guterch, A., Banka, D., Lamarche, J., Lassen, A., Lewerenz, B., Scheck, M., Marotta, A.M., 2002. The southern margin of the East European Craton: New results from seismic sounding and potential fields between the North Sea and Poland. Tectonophysics 360, 301–314.

Betts, P.G., Giles, D., 2006. The 1800-1100 Ma tectonic evolution of Australia. Precambrian Research 144, 92–125.

Black, R., Liegeois, J.P., 1993. Cratons, mobile belts, alkaline rocks and continental lithospheric mantle: the Pan-African testimony. Journal of the Geological Society, London 150, 89–98.

Bostock, M.G., 2013. The Moho in subduction zones. Tectonophysics 609, 547–557.

Bostock, M.G., Hyndman, R.D., Rondenay, S., Peacock, S.M., 2002. An inverted continental Moho and serpentinization of the forearc mantle. Nature 417, 536–538.

Cawood, P.A., Korsch, R.J., 2008. Assembling Australia: Proterozoic building of a continent. Precambrian Research 166, 1–35.

Cawood, P.A., Kroner, A., Collins, W.J., Kusky, T.M., Mooney, W.D., Windley, B.F., 2009. Accretionary orogens through Earth history. Geological Society, London, Special Publications 318, 1–36.

Chen, Y., Niu, F., Liu, R., Huang, Z., Tkalčič, H., Sun, L., Chan, W., 2010. Crustal structure beneath China from receiver function analysis. Journal of Geophysical Research 115, 1–22.

Chevrot, S., van der Hilst, R., 2000. The Poisson ratio of the Australian crust: Geological and geophysical implications. Earth and Planetary Science Letters 183, 121–132.

Clark, C., Kirkland, C.L., Spaggiari, C.V., Oorschot, C., Wingate, M., Taylor, R.J., 2014. Proterozoic granulite formation driven by mafic magmatism: An example from the Fraser Range Metamorphics, Western Australia. Precambrian Research 240, 1–21.

Clark, D.J., Hensen, B.J., Kinny, P.D., 2000. Geochronological constraints for a two-stage history of the Albany-Fraser Orogen, Western Australia. Precambrian Research 102, 155–183.

Clitheroe, G., Gudmundsson, O., Kennett, B.L.N., 2000. The crustal thickness of Australia. Journal of Geophysical Research 105, 13697.

Collins, C., Drummond, B.J., Nicoll, M., 2003. Crustal thickness patterns in the Australian continent. Geological Society of America Special Papers 372, 121–128.

Condie, K.C., Myers, J.S., 1999. Mesoproterozoic Fraser Complex: Geochemical evidence for multiple subduction-related sources of lower crustal rocks in the Albany-Fraser Orogen, Western Australia. Australian Journal of Earth Sciences 46, 875–882.

Crotwell, H.P., Owens, T.J., 2005. Automated Receiver Function Processing. Seismological Research Letters 76, 702–709.

Durrheim, R.J., Mooney, W.D., 1991. Archean and Proterozoic crustal evolution: evidence from crustal seismology. Geology 19, 606–609.

Fitzsimons, I.C.W., 2003. Proterozoic basement provinces of southern and southwestern Australia, and their correlation with Antarctica. Geological Society, London, Special Publications 206, 93–130.

Fletcher, I.R., Myers, J.S., Ahmat, A.L., 1991. Isotopic evidence on the age and origin of the Fraser Complex, Western Australia: a sample of Mid-Proterozoic lower crust. Chemical Geology: Isotope Geoscience Section 87, 197–216.

Ford, H., Fischer, K.M., Abt, D.L., Rychert, C.A., Elkins-Tanton, L.T., 2010. The lithosphere-asthenosphere boundary and cratonic lithospheric layering beneath Australia from Sp wave imaging. Earth and Planetary Science Letters 300, 299–310.

Fraser, A.R., Pettifer, G.R., 1980. Reconnaissance gravity surveys in Western Australia and South Australia, 1969-1972. Bureau of Mineral Resources Bulletin 196, 1969–1972.

Gibb, R.A., Thomas, M.D., 1976. Gravity signature of fossil plate boundaries in the Canadian Shield. Nature 262, 774–776.

Gibb, R.A., Thomas, M.D., Lapointe, P.L., Mukhopadhyay, M., 1983. Geophysics of proposed proterozoic sutures in Canada.

Precambrian Research 19, 349–384.

Giles, D., Betts, P.G., Lister, G.S., 2004. 1.8-1.5-Ga links between the North and South Australian Cratons and the Early-Middle Proterozoic configuration of Australia. Tectonophysics 380, 27–41.

Gilligan, A., Bastow, I.D., Darbyshire, F.A., 2016. Seismological structure of the 1.8 Ga Trans-Hudson Orogen of North America. Geochemistry, Geophysics, Geosystems 17, 2421–2433.

Goleby, B.R., Blewett, R.S., Fomin, T., Fishwick, S., Reading, A.M., Henson, P.A., Kennett, B.L.N., Champion, D.C., Jones, L., Drummond, B.J., Nicoll, M., 2006. An integrated multi-scale 3D seismic model of the Archaean Yilgarn Craton, Australia. Tectonophysics 420, 75–90.

Gorbatov, A., Saygin, E., Kennett, B.L.N., 2013. Crustal properties from seismic station autocorrelograms. Geophysical Journal International 192, 861–870.

Guillot, S., Hattori, K.H., De Sigoyer, J., 2000. Mantle wedge serpentinization and exhumation of eclogites: Insights from eastern Ladakh, northwest Himalaya. Geology 28, 199–202.

Gurnis, M., 1998. Cretaceous Vertical Motion of Australia and the AustralianAntarctic Discordance. Science 279, 1499–1504.

Hajnal, Z., Lewry, J., White, D., Ashton, K., Clowes, R., Stauffer, M., Gyorfi, I., Takacs, E., 2005. The Sask Craton and Hearne Province margin: seismic reflection studies in the western Trans-Hudson Orogen. Canadian Journal of Earth Sciences 42, 403–419.

James, D.E., Fouch, M.J., 2002. Formation and evolution of Archaean cratons: insights from southern Africa. Geological Society, London, Special Publications 199, 1–26.

Johnson, S.P., Sheppard, S., Rasmussen, B., Wingate, M., Kirkland, C.L., Muhling, J.R., Fletcher, I.R., Belousova, E.A., 2011. Two collisions, two sutures: Punctuated pre-1950Ma assembly of the West Australian Craton during the Ophthalmian and Glenburgh Orogenies. Precambrian Research 189, 239–262.

Kennett, B.L.N., Engdahl, E.R., Buland, R., 1995. Constraints on seismic velocities in the Earth from travel times. Geophysical Journal International 122, 108–124.

Kennett, B.L.N., Iaffaldano, G., 2013. Role of lithosphere in intra-continental deformation: Central Australia. Gondwana Research 24, 958–968.

Kennett, B.L.N., Salmon, M., Saygin, E., Group, A.W., 2011. AusMoho: The variation of Moho depth in Australia. Geophysical Journal International 187, 946–958.

Kennett, B.L.N., Saygin, E., 2015. The nature of the Moho in Australia from reflection profiling: A review. GeoResJ 5, 74–91.

Kennett, B.L.N., Saygin, E., Salmon, M., 2015. Stacking autocorrelograms to map Moho depth with high spatial resolution in southeastern Australia. Geophysical Research Letters 42, 7490–7497.

Kennett, B.L.N., Yoshizawa, K., 2016. Lithospheric discontinuities beneath Australia: interaction of large-scale and fine scale structure, in: Geophysical Research Abstracts, p. EGU General Assembly.

Kirkland, C.L., Smithies, R.H., Spaggiari, C.V., 2014. Foreign contemporaries - Unravelling disparate isotopic signatures from Mesoproterozoic Central and Western Australia. Precambrian Research 265, 1–14.

Kirkland, C.L., Spaggiari, C.V., Pawley, M., Wingate, M., Smithies, R.H., Howard, H., Tyler, I.M., Belousova, E.A., Poujol, M., 2011. On the edge: U-Pb, Lu-Hf, and Sm-Nd data suggests reworking of the Yilgarn craton margin during formation of the Albany-Fraser Orogen. Precambrian Research 187, 223–247.

Korsch, R.J., Huston, D.L., Henderson, R.A., Blewett, R.S., Withnall, I.W., Fergusson, C.L., Collins, W.J., Saygin, E., Kositcin, N., Meixner, A.J., Chopping, R., Henson, P.A., Champion, D.C., Hutton, L.J., Wormald, R., Holzschuh, J., Costelloe, R.D., 2012. Crustal architecture and geodynamics of North Queensland, Australia: Insights from deep seismic reflection profiling. Tectonophysics 572-573, 76–99.

Korsch, R.J., Spaggiari, C.V., Occhipinti, S., Doublier, M.P., Clark, D.J., Dentith, M.C., Doyle, M., Kennett, B.L.N., Gessner, K., Neumann, N., Belousova, E.A., Tyler, I.M., Costelloe, R.D., Fomin, T., Holzschuh, J., 2014. Geodynamic implications of the 2012 Albany-Fraser deep seismic reflection survey: a transect from the Yilgarn Craton across the Albany-Fraser Orogen to the Madura Province, in: Spaggiari, C.V., Tyler, I.M. (Eds.), Albany-Fraser Orogen Seismic and Magnetotelluric (MT) workshop 2014: extended abstracts. Geological Survey of Western Australia, Perth, Record 2014/06, pp. 142–173.

Lenardic, A., Moresi, L., Mühlhaus, H., 2000. The role of mobile belts for the longevity of deep cratonic lithosphere: The crumple zone model. Geophysical Research Letters 27, 1235–1238.

Lewry, J., Hajnal, Z., Green, A., Lucas, S.B., White, D., Stauffer, M., Ashton, K., Weber, W., Clowes, R., 1994. Structure of a Paleoproterozoic continent-continent collision zone: a LITHOPROBE seismic reflection profile across the Trans-Hudson Orogen, Canada. Tectonophysics 232, 143–160.

Ligorría, J.P., Ammon, C.J., 1999. Iterative deconvolution and receiver-function estimation. Bulletin of the Seismological Society of America 89, 1395–1400.

Maier, W.D., Smithies, R.H., Spaggiari, C.V., Barnes, S.J., Kirkland, C.L., Kiddle, O., Roberts, M., 2016a. The evolution of mafic and ultramafic rocks of the Mesoproterozoic Fraser Zone, Albany-Fraser Orogen, and implications for Ni-Cu sulfide potential of the region. Technical Report. Geological Survey of Western Australia. Perth, Record 2016/08.

Maier, W.D., Smithies, R.H., Spaggiari, C.V., Barnes, S.J., Kirkland, C.L., Yang, S., Lahaye, Y., Kiddie, O., MacRae, C., 2016b. Petrogenesis and Ni-Cu sulphide potential of mafic-ultramafic rocks in the Mesoproterozoic Fraser Zone within the Albany-Fraser Orogen, Western Australia. Precambrian Research 281, 27–46.

Meissner, R., 1989. Rupture, creep, lamellae and crocodiles: happenings in the continental crust. Terra Nova 1, 17–28.

Mercier, J.P., Bostock, M.G., Audet, P., Gaherty, J.B., Garnero, E.J., Revenaugh, J., 2008. The teleseismic signature of fossil subduction: Northwestern Canada. Journal of Geophysical Research: Solid Earth 113, 1–16.

Mjelde, R., Goncharov, A., Müller, R.D., 2013. The Moho: Boundary above upper mantle peridotites or lower crustal eclogites? A global review and new interpretations for passive margins. Tectonophysics 609, 636–650.

Mooney, W.D., Laske, G., Masters, T.G., 1998. CRUST 5.1: A global crustal model at 5 5. Journal of Geophysical Research 103, 727–747.

Moore, V.M., Wiltschko, D.V., 2004. Syncollisional delamination and tectonic wedge development in convergent orogens. Tectonics 23, TC2005.

Murdie, R., Gessner, K., Occhipinti, S., Spaggiari, C.V., Brett, J., 2014. Interpretation of gravity and magnetic data across the Albany-Fraser Orogen, in: Spaggiari, C.V., Tyler, I.M. (Eds.), Albany-Fraser Orogen Seismic and Magnetotelluric (MT) workshop 2014: extended abstracts. Geological Survey of Western Australia, Perth, Record 2014/06, pp. 118–134.

Myers, J.S., 1990. Precambrian tectonic evolution of part of Gondwana, southwestern Australia. Geology 18, 537–540.

Myers, J.S., 1993. Precambrian History of the West Australian Craton and adjacent orogens. Annual Reviews of Earth and Planetary Sciences 21, 453–485.

Myers, J.S., Shaw, R.D., Tyler, I.M., 1996. Tectonic evolution of Proterozoic Australia. Tectonics 15, 1431–1446.

Nguuri, T.K., Gore, J., James, D.E., Webb, S.J., Wright, C., Zengeni, T.G., Gwavava, O., Snoke, J.A., 2001. Crustal structure beneath southern Africa and its implications for the formation and evolution of the Kaapvaal and Zimbabwe cratons. Geophysical Research Letters 28, 2501–2504.

Occhipinti, S., Doyle, M., Spaggiari, C.V., Korsch, R.J., Cant, G., Martin, K., Kirkland, C.L., Savage, J., Less, T., Bergin, L., Fox, L., 2014. Interpretation of the deep seismic reflection line 12GA-T1: northeast Albany-Fraser Orogen, in: Spaggiari, C.V., Tyler, I.M. (Eds.), Albany-Fraser Orogen Seismic and Magnetotelluric (MT) workshop 2014: extended abstracts. Geological Survey of Western Australia, Perth, Record 2014/06, pp. 52–68.

Occhipinti, S., Tyler, I.M., Spaggiari, C.V., Korsch, R.J., Kirkland, C.L., Smithies, R.H., Martin, K., Wingate, M., 2016. Tropicana translated - a forelast thrust system imbricate fan setting for c. 2520 Ma gold mineralization at the northern margin of the Albany-Fraser Orogen, Western Australia. Geological Society, London, Special Publications in press.

Oxburgh, E.R., 1972. Flake Tectonics and Continental Collision. Nature 239, 202–204.

Pearce, D., Rondenay, S., Sachpazi, M., Charalampakis, M., Royden, L.H., 2012. Seismic investigation of the transition from continental to oceanic subduction along the western Hellenic subduction Zone. Journal of Geophysical Research 117, 1–18.

Poudjom Djomani, Y.H., O'Reilly, S.Y., Griffin, W.L., Morgan, P., 2001. The density structure of subcontinental lithosphere through time. Earth and Planetary Science Letters 184, 605–621.

Reading, A.M., Kennett, B.L.N., Dentith, M.C., 2003. Seismic structure of the Yilgarn Craton , Western Australia. Australian Journal of Earth Sciences 50, 427–438.

Reading, A.M., Kennett, B.L.N., Goleby, B.R., 2007. New constraints on the seismic structure of West Australia: Evidence for terrane stabilization prior to the assembly of an ancient continent? Geology 35, 379–382.

Salmon, M., Kennett, B.L.N., Saygin, E., 2013. Australian Seismological Reference Model (AuSREM): crustal component. Geophysical Journal International 192, 190–206.

Schneider, F.M., Yuan, X., Schurr, B., Mechie, J., Sippl, C., Haberland, C., Minaev, V., Oimahmadov, I., Gadoev, M., Radjabov, N., Abdybachaev, U., Orunbaev, S., Negmatullaev, S., 2013. Seismic imaging of subducting continental lower crust beneath the Pamir. Earth and Planetary Science Letters 375, 101–112.

Scott, D.L., Rawlings, D.J., Page, R.W., Tarlowski, C.Z., Idnurm, M., Jackson, M.J., Southgate, P.N., 2000. Basement framework and geodynamic evolution of the Palaeoproterozoic superbasins of north-central Australia: An integrated review of geochemical, geochronological and geophysical data. Australian Journal of Earth Sciences 47, 341–380.

Sippl, C., 2016. Moho geometry along a north-south passive seismic transect through Central Australia. Tectonophysics 676, 56–69.

Sippl, C., Kennett, B.L.N., Tkalčič, H., Spaggiari, C.V., Gessner, K., 2015. New constraints on the current stress field and seismic velocity structure of the eastern Yilgarn Craton from mechanisms of local earthquakes. Australian Journal of Earth Sciences 62, 921–931.

Smithies, R.H., Spaggiari, C.V., Kirkland, C.L., 2015. Building the crust of the AlbanyFraser Orogen; constraints from granite geochemistry. Technical Report. Geological Survey of Western Australia Report 150. Perth.

Smithies, R.H., Spaggiari, C.V., Kirkland, C.L., Maier, W.D., 2014. Geochemistry and petrogenesis of igneous rocks in the Albany-Fraser Orogen, in: Spaggiari, C.V., Tyler, I.M. (Eds.), Albany-Fraser Orogen Seismic and Magnetotelluric (MT) workshop 2014: extended abstracts. Geological Survey of Western Australia, Perth, Record 2014/06, pp. 69–80.

Snyder, D.B., Goleby, B.R., 2016. Seismic reflection patterns associated with continental convergent margins through time. Tectonophysics in press.

Spaggiari, C.V., 2016. Interpreted bedrock geology of the East Albany-Fraser Orogen: East Albany-Fraser Orogen 2016. Technical Report. Geological Survey of Western Australia, Geological Exploration Package. Perth.

Spaggiari, C.V., Kirkland, C.L., Smithies, R.H., Occhipinti, S., Wingate, M., 2014a. Geological framework of the Albany-Fraser Orogen, in: Spaggiari, C.V., Tyler, I.M. (Eds.), Albany-Fraser Orogen Seismic and Magnetotelluric (MT) workshop 2014: extended abstracts. Geological Survey of Western Australia, Perth, Record 2014/06, pp. 12–27.

Spaggiari, C.V., Kirkland, C.L., Smithies, R.H., Wingate, M., Belousova, E.A., 2015. Transformation of an Archean craton margin during Proterozoic basin formation and magmatism: The AlbanyFraser Orogen, Western Australia. Precambrian Research 266, 440–466.

Spaggiari, C.V., Occhipinti, S., 2014. Geological interpretation of the Albany-Fraser Orogen and southeast Yilgarn Craton seismic lines, 12GA-AF1, 12GA-AF2, 12GA-AF3 and 12GA-T1 (1:500 000 scale), in: Spaggiari, C.V., Tyler, I.M. (Eds.), Albany-Fraser Orogen Seismic and Magnetotelluric (MT) workshop 2014: extended abstracts. Geological Survey of Western Australia, Perth, Record 2014/06, p. Plate 4.

Spaggiari, C.V., Occhipinti, S., Korsch, R.J., Doublier, M.P., Clark, D.J., Dentith, M.C., Gessner, K., Doyle, M., Tyler, I.M., Kennett, B.L.N., Costelloe, R.D., Fomin, T., Holzschuh, J., 2014b. Interpretation of Albany-Fraser seismic lines 12GA-AF1, 12GA-AF2 and 12 GA-AF3: implications for crustal architecture, in: Spaggiari, C.V., Tyler, I.M. (Eds.), Albany-Fraser

Orogen Seismic and Magnetotelluric (MT) workshop 2014: extended abstracts. Geological Survey of Western Australia, Perth, Record 2014/06, pp. 28–51.

Spaggiari, C.V., Smithies, R.H., 2015. Eucla Basement Stratigraphic Drilling Results Release Workshop: Extended Abstracts. Geological Survey of Western Australia, Perth, Record 2015/10.

Swager, C.P., 1997. Tectono-stratigraphy of late Archaean greenstone terranes in the southern Eastern Goldfields, Western Australia. Precambrian Research 83, 11–42.

Tassell, H., Goncharov, A., 2006. Geophysical evidence for a deep crustal root beneath the Yilgarn Craton and the Albany-Fraser Orogen, in: AESC Conference 2006, Extended Abstracts.

Teixell, A., 1998. Crustal structure and orogenic material budget in the west central Pyrenees. Tectonics 17, 395–406.

TRANSALP_working_group, 2002. First deep seismic reflection images of the Eastern Alps reveal giant crustal wedges and transcrustal ramps. Geophysical Research Letters 29, 1–4.

Tyler, I.M., Thorne, A.M., 1990. The northern margin of the Capricorn Orogen, Western Australia-an example of an Early Proterozoic collision zone. Journal of Structural Geology 12, 685–701.

de Vries, S.T., Pryer, L., Fry, N., 2008. Evolution of Neoarchaean and Proterozoic basins of Australia. Precambrian Research 166, 39–53.

Wellman, P., 1978. Gravity evidence for abrupt changes in mean crustal density at the junction of Australian crustal blocks. BMR Journal of Australian Geology & Geophysics 3, 153–162.

Wittlinger, G., Farra, V., Hetényi, G., Vergne, J., Nábělek, J., 2009. Seismic velocities in Southern Tibet lower crust: A receiver function approach for eclogite detection. Geophysical Journal International 177, 1037–1049.

Yin, A., Harrison, T.M., 2000. Geologic Evolution of the Himalayan-Tibetan orogen. Annual Reviews of Earth and Planetary Sciences 28, 211–280.

Yoshizawa, K., 2014. Radially anisotropic 3-D shear wave structure of the Australian lithosphere and asthenosphere from multi-mode surface waves. Physics of the Earth and Planetary Interiors 235, 33–48.

Youssof, M., Thybo, H., Artemieva, I.M., Levander, A., 2013. Moho depth and crustal composition in Southern Africa. Tectonophysics 609, 267–287.

Yuan, H., 2015. Secular change in Archaean crust formation recorded in Western Australia. Nature Geoscience 8, 808–813.

Zhang, S., Gao, R., Li, H., Hou, H., Wu, H., Li, Q., Yang, K., Li, C., Li, W., Zhang, J., Yang, T., Keller, G.R., Liu, M., 2014. Crustal structures revealed from a deep seismic reflection profile across the Solonker suture zone of the Central Asian Orogenic Belt, northern China: An integrated interpretation. Tectonophysics 612-613, 26–39.

Zhu, L., Kanamori, H., 2000. Moho depth variation in southern California from teleseismic receiver functions, J. Journal of Geophysical Research 105, 2969–2980.

Figure 1.

A) Interpreted bedrock geology map of the Eastern Albany-Fraser Orogen and surrounding areas (after Spaggiari et al., 2015). Triangles and squares mark the positions of seismic stations used in this study (triangles: short-period stations; squares: broadband stations). Blue symbols refer to the first installation phase of the ALFREX array from 11/2013 to 09/2014, red symbols to the second installation phase (09/2014 to 01/2016), green and orange symbols mark permanent stations and stations from the different WACraton deployments (e.g. Reading et al., 2007), respectively. Red lines mark the location of active seismic profiles 12GA-AF1, 12GA-AF2 and 12GA-AF3, acquired in 2012, dark blue lines show the position of the CCP and gravity modelling profiles shown in Figures 6 and 8. B) Overview surface geology map of Western Australia that shows the position of the study region displayed in subfigures A and C as a red box (modified after Cawood and Korsch, 2008). YC - Yilgarn Craton, PO - Pinjarra Orogen, AFO - Albany-Fraser Orogen, EB - Eucla Basin. C) Bouguer gravity map of the study area, with seismic stations shown as red dots. This plot shows the same area as subfigure A.

Figure 2.

Visualizations of receiver function variation for single stations, which most likely derives from Moho topography underneath. A) Inner quartile ranges (a measure of distribution width) of handpicked Ps-P times for receiver functions of each station, plotted onto a regional map. Two stations, FD52 and FD64, with anomalously large inner quartile ranges of above 0.7 seconds (marked with red rings) were investigated in more detail in subfigure B. Contour lines of the crustal thickness map derived from H-K stacking (Figure 3) are overlain. It can be seen that inner quartile ranges are small where the Moho is horizontal and largest where significant gradients in Moho depth are present, especially around the western edge of the Moho trough we obtain. B) Polar plots of the single Ps-P times of stations FD52 and FD64, plotted at their piercing points (backazimuth angles and piercing distances from the station in km). Both stations show clear trends of systematically variable delay times for different azimuth angles, and these trends oppose each other, which is due to the positions of these stations on opposite edges of the Moho trough.

Figure 3.

Crustal thickness (A) and v_p/v_s (B) maps retrieved from H-K stacking. Colored circles mark the retrieved values at the different stations; the map between these points is interpolated. Stations with bold circle outlines are sites for which receiver function analysis did not succeed (see Examples in Figure S5) and for which a crustal thickness estimate was obtained from autocorrelograms (Figure S6); there are no v_p/v_s values for these sites. Blue and red contours outline negative and positive gravity anomalies, respectively (see Figure 1C).

Figure 4.

A) 1534 crustal thickness values derived for single receiver functions and plotted at their calculated Moho piercing point. Moho picks from the three active seismic profiles (12GA-AF1 to 12GA-AF3) are also included. B) Interpolated crustal thickness map from these point measurements. Black lines correspond to faults, shear zones and unit boundaries shown in Figure 1A. In comparison to Figure 3A, the southern (narrower) part of the Moho trough shows up more prominently.

Figure 5.

A) Contours of the crustal thickness map derived from Ps-P times at Moho piercing points (Figure 4) plotted in blue onto the regional geology map (Figure 1A). Profiles A-A' to C-C' show the location of the CCP profiles shown in Figure 6, with the stations utilized for the profiles plotted in the same colors as the profile lines. Seismic stations shown as grey circles were not used for the CCP profiles. Lines 12GA-AF1 to 12GA-AF3 show the location of the three active seismic profiles (Figure 7). B) Crustal thickness contours overlain onto Bouguer gravity map (as in Figure 1C). Other plot elements as in subfigure A.

Figure 6.

Three common conversion point (CCP) profiles through the study area, oriented perpendicular to the strike of the main geological units. For location of the single profiles refer to Figure 5. The approximate position of faults/shear zones and the main geological units are given above the profile. Structures in grey color are not intersected by the profile, but occur within the projection width of some stations. The Moho is visible as the most prominent negative (red) phase throughout all profiles and is marked with a dashed line (dotted line where uncertain). CSZ - Cundeelee Shear Zone, FSZ - Fraser Shear Zone, CRSZ - Coramup Shear Zone, NSZ - Newman Shear Zone, JF - Jerdacuttup Fault.

Figure 7.

Moho depth from our interpolated map (red dashed lines; from Figure 4) projected on the geological interpretation of the three active seismic profiles 12 GA-AF1-3 (see Figure 5 for location). Note that differences in crustal thickness are small and the general shape of the Moho is well matched by our study. Modified from Spaggiari et al. (2014b).

Figure 8.

Crustal density models along profiles 12GA-AF3 (upper left), A-A' (lower left), B-B' (upper right), C-C' (center right) and 12GA-AF1+2 (lower right). For each profile, the uppermost panel shows the observed and modelled gravity anomaly values, the center panel shows the utilized density distributions and the lower panel the corresponding geological units. For the location of the profiles, refer to Figures 1 and 5. "Moho model" refers to a configuration with uniform density crust (2.67 g/cm^3) overlying a uniform mantle (3.2 g/cm^3). Moho geometries are taken from the CCP profiles (Figure 6) for profiles A-A', B-B' and C-C', or from the active seismic profiles for 12GA-AF3 and 12GA-AF1+2. Lithological units were likewise taken from the active seismic profile interpretations (Spaggiari et al., 2014b) or extrapolated between those. Regions with the same inferred lithology are given the same density along strike. Nomenclature of shear zones and faults as in Figures 1A and 6.

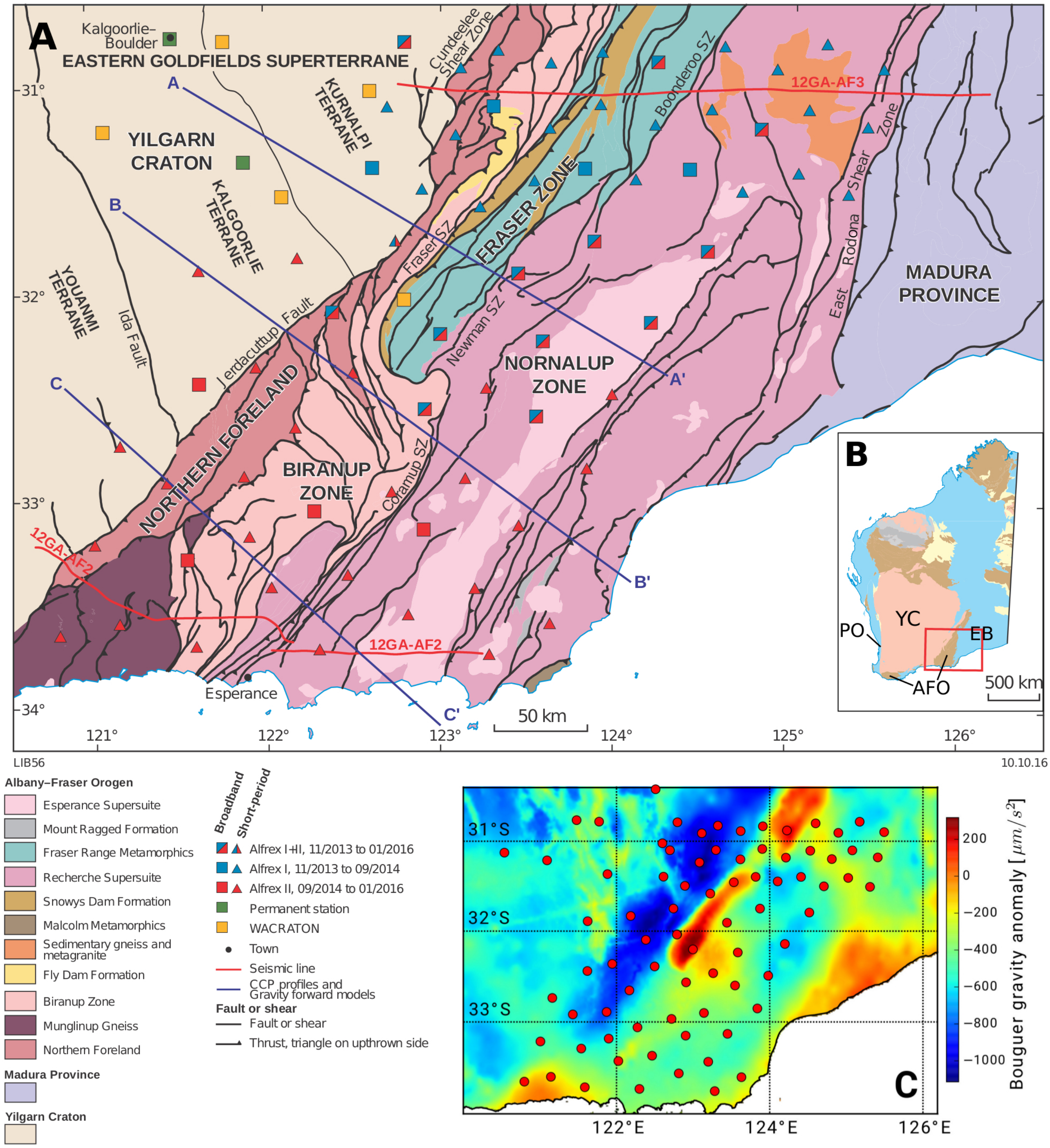
A
Kalgoorlie–Boulder
EASTERN GOLDFIELDS SUPERTERRANE
YILGARN CRATON
KURNALPI TERRANE
KALGOORLIE TERRANE
YOUANMI TERRANE
Ida Fault
Jerdacuttup Fault
NORTHERN FORELAND
BIRANUP ZONE
NORNALUP ZONE
FRASER ZONE
MADURA PROVINCE
Cundeelee Shear Zone
Fraser SZ
Newman SZ
Boonderoo SZ
Coramup SZ
East Rodona Shear Zone
12GA-AF3
12GA-AF2
Esperance
50 km
A
A'
B
B'
C
C'
31°
32°
33°
34°
121°
122°
123°
124°
125°
126°
B
YC
PO
EB
AFO
500 km
LIB56
10.10.16
Albany–Fraser Orogen
Esperance Supersuite
Mount Ragged Formation
Fraser Range Metamorphics
Recherche Supersuite
Snowys Dam Formation
Malcolm Metamorphics
Sedimentary gneiss and metagranite
Fly Dam Formation
Biranup Zone
Munglinup Gneiss
Northern Foreland
Madura Province
Yilgarn Craton
Broadband
Short-period
Alfrex I+II, 11/2013 to 01/2016
Alfrex I, 11/2013 to 09/2014
Alfrex II, 09/2014 to 01/2016
Permanent station
WACRATON
Town
Seismic line
CCP profiles and Gravity forward models
Fault or shear
Fault or shear
Thrust, triangle on upthrown side
31°S
32°S
33°S
122°E
124°E
126°E
C
200
0
−200
−400
−600
−800
−1000
Bouguer gravity anomaly [$\mu m/s^2$]

Figure 1:

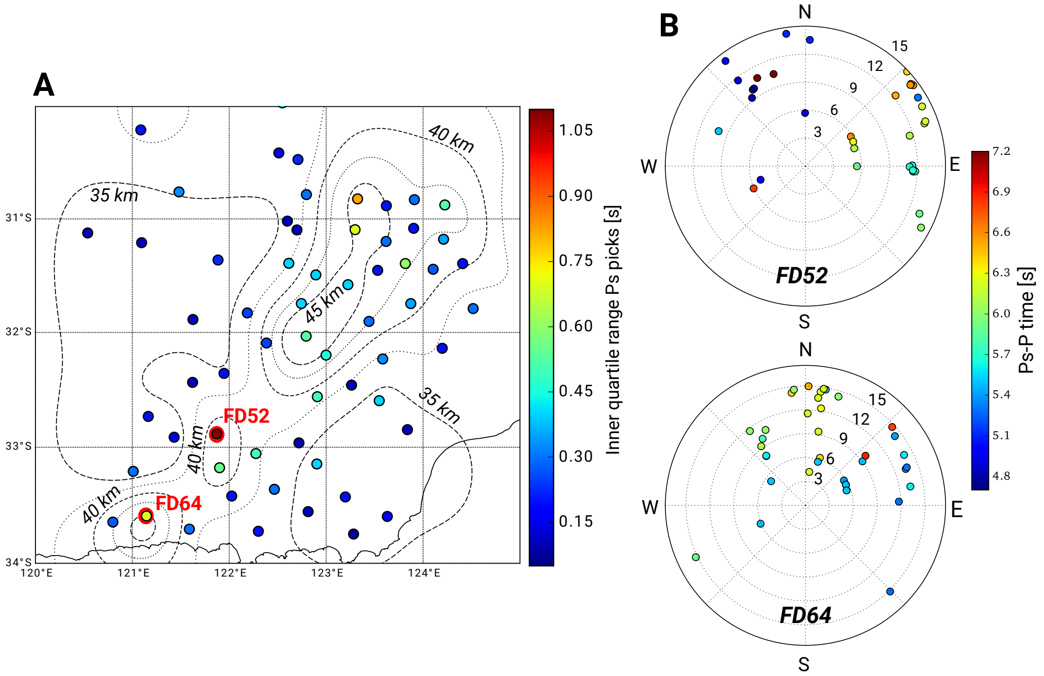

Figure 2:

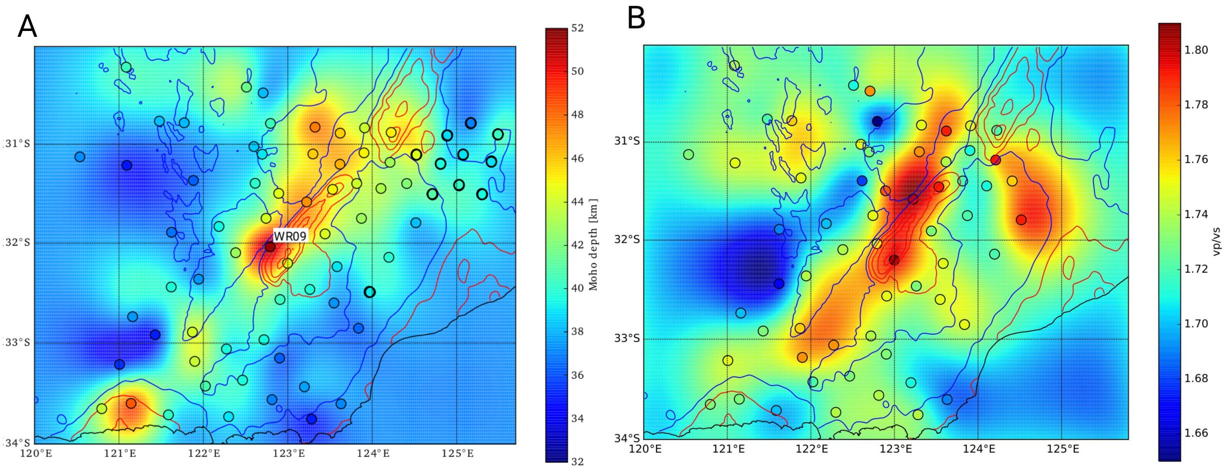

Figure 3:

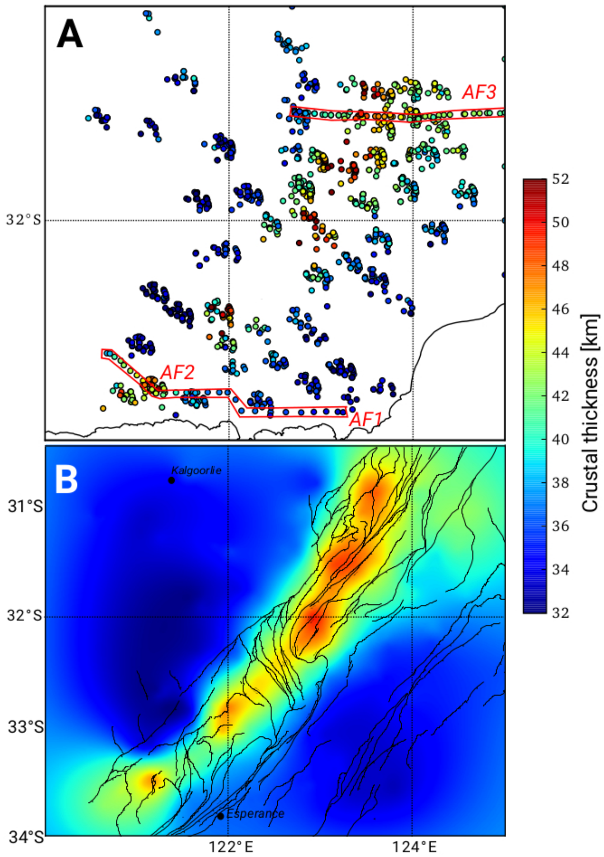

A
AF3
AF2
AF1
32°S
B
Kalgoorlie
Esperance
31°S
32°S
33°S
34°S
122°E
124°E
52
50
48
46
44
42
40
38
36
34
32
Crustal thickness [km]

Figure 4:

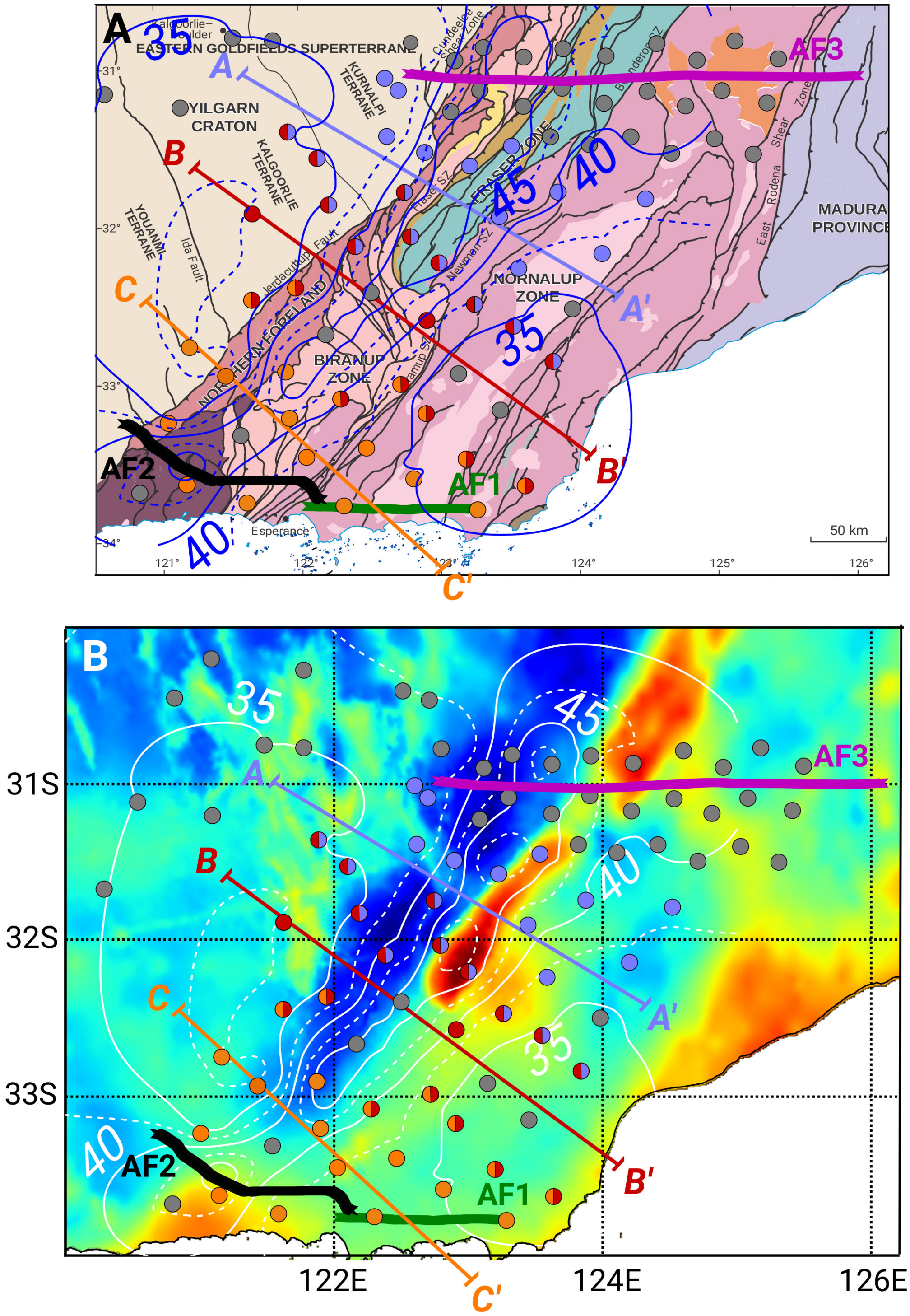
A
B
EASTERN GOLDFIELDS SUPERTERRANE
YILGARN CRATON
KURNALPI TERRANE
KALGOORLIE TERRANE
YOUANMI TERRANE
NORTHERN FORELAND
FRASER ZONE
BIRANUP ZONE
NORNALUP ZONE
MADURA PROVINCE
Esperance
AF1
AF2
AF3
50 km
31S
32S
33S
122E
124E
126E

Figure 5:

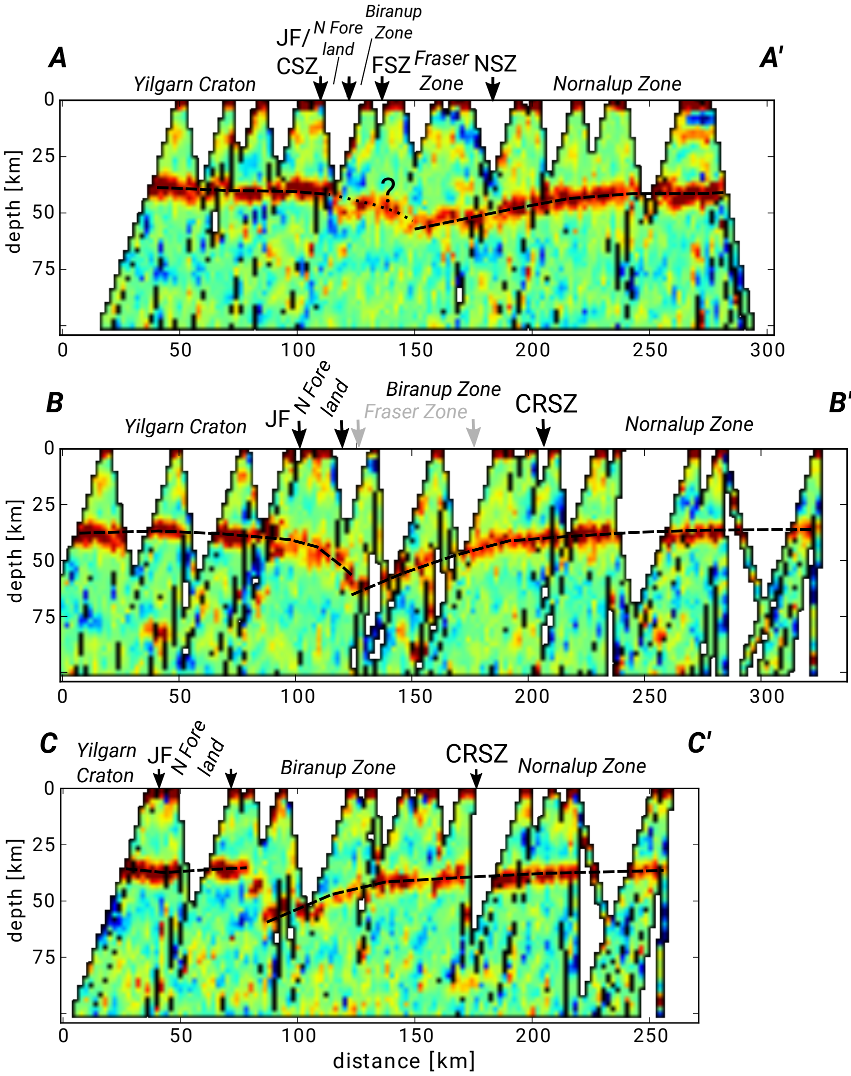

A
A′
Yilgarn Craton
JF/
CSZ
N Fore
land
Biranup
Zone
FSZ
Fraser
Zone
NSZ
Nornalup Zone
?
depth [km]
B
B′
Yilgarn Craton
JF
N Fore
land
Biranup Zone
Fraser Zone
CRSZ
Nornalup Zone
C
C′
Yilgarn
Craton
JF
N Fore
land
Biranup Zone
CRSZ
Nornalup Zone
distance [km]

Figure 6:

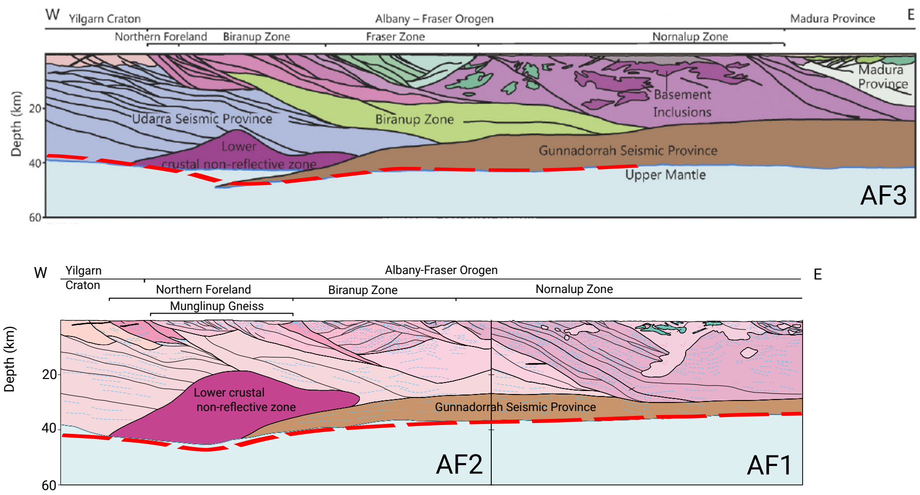
W
Yilgarn Craton
Albany – Fraser Orogen
Madura Province
E
Northern Foreland
Biranup Zone
Fraser Zone
Nornalup Zone
Depth (km)
20
40
60
Madura Province
Basement Inclusions
Udarra Seismic Province
Biranup Zone
Lower crustal non-reflective zone
Gunnadorrah Seismic Province
Upper Mantle
AF3
W
Yilgarn Craton
Albany-Fraser Orogen
E
Northern Foreland
Munglinup Gneiss
Biranup Zone
Nornalup Zone
Depth (km)
20
40
60
Lower crustal non-reflective zone
Gunnadorrah Seismic Province
AF2
AF1

Figure 7:

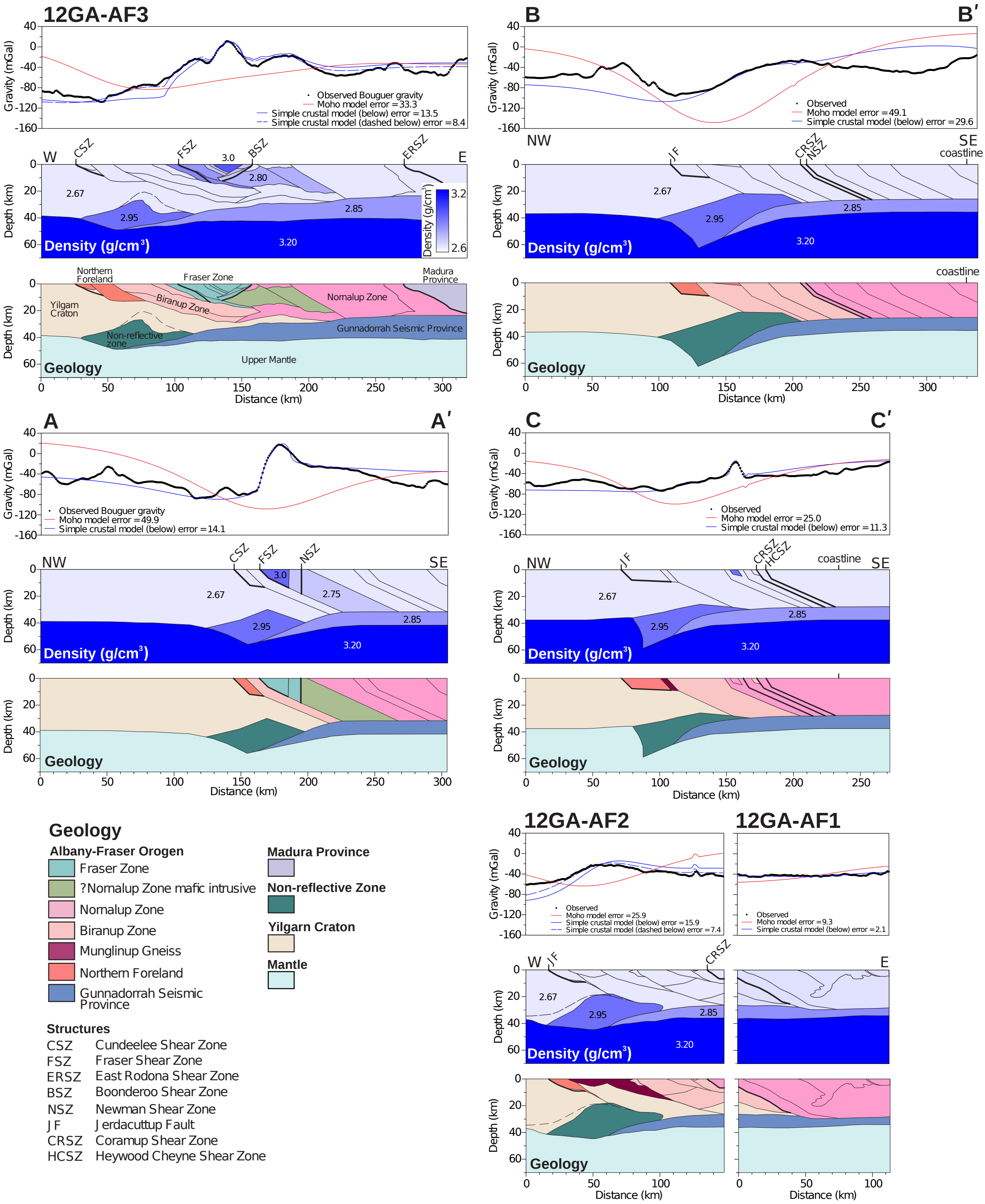
12GA-AF3
B
B′
A
A′
C
C′
12GA-AF2
12GA-AF1
Gravity (mGal)
Depth (km)
Distance (km)
Observed Bouguer gravity
Observed
Moho model error
Simple crustal model (below) error
Simple crustal model (dashed below) error
Density (g/cm³)
Geology
W
E
NW
SE
coastline
CSZ
FSZ
BSZ
ERSZ
NSZ
JF
CRSZ
HCSZ
Northern Foreland
Fraser Zone
Madura Province
Yilgarn Craton
Biranup Zone
Nornalup Zone
Non-reflective zone
Gunnadorrah Seismic Province
Upper Mantle
Geology
Albany-Fraser Orogen
Fraser Zone
?Nornalup Zone mafic intrusive
Nornalup Zone
Biranup Zone
Munglinup Gneiss
Northern Foreland
Gunnadorrah Seismic Province
Madura Province
Non-reflective Zone
Yilgarn Craton
Mantle
Structures
CSZ Cundeelee Shear Zone
FSZ Fraser Shear Zone
ERSZ East Rodona Shear Zone
BSZ Boonderoo Shear Zone
NSZ Newman Shear Zone
JF Jerdacuttup Fault
CRSZ Coramup Shear Zone
HCSZ Heywood Cheyne Shear Zone

Figure 8: